(2)

UNIVERSITY OF CALIFORNIA, BERKELEY

BERKELEY • DAVIS • IRVINE • LOS ANGELES • RIVERSIDE • SAN DIEGO • SAN FRANCISCO | SANTA BARBARA • SANTA CRUZ

SEISMOGRAPHIC STATION
DEPARTMENT OF GEOLOGY AND GEOPHYSICS

BERKELEY, CALIFORNIA 94720

28 February 1985

Air Force Office of Scientific Research
Attention: NP
Bolling Air Force Base
Washington, D.C. 20332

FINAL REPORT

ARPA Order No. 4397/3
Program Code 3D60
Grantee: The Regents of the University of California
Effective Date of Grant: 01 October 1982
Grant Termination Date: 31 December 1984
Amount of Grant: $250,000
Grant No. AFOSR-F49620-83-C-0020
Principal Investigators: T. V. McEvilly (415) 642-4494
L. R. Johnson (414) 642-1275
Program Manager: William J. Best (202) 693-0162

Short Title of Work: REGIONAL STUDIES WITH BROADBAND DATA

T. V. McEvilly

Lane Johnson
L. R. Johnson

Sponsored by
Advanced Research Projects Agency (DOD)
ARPA Order No. 4397/3
Monitored by AFOSR Under Contract No. F49620-83-C-0020

Blank Page

UNCLASSIFIED

SECURITY CLASSIFICATION OF THIS PAGE (When Data Entered)

REPORT DOCUMENTATION PAGE		READ INSTRUCTIONS BEFORE COMPLETING FORM
1. REPORT NUMBER AFOSR-TR- 85-0889 ~~Final Report~~	2. GOVT ACCESSION NO. AD-A161497	3. RECIPIENT'S CATALOG NUMBER
4. TITLE (and Subtitle) Regional Studies with Broadband Data		5. TYPE OF REPORT & PERIOD COVERED Final Report 01 Oct 1983 - 31 Dec 1984
		6. PERFORMING ORG. REPORT NUMBER
7. AUTHOR(s) T. V. McEvilly, L. R. Johnson		8. CONTRACT OR GRANT NUMBER(s) AFOSR-F49620-83-C0020
9. PERFORMING ORGANIZATION NAME AND ADDRESS Seismographic Station, University of California, Berkeley, California 94720		10. PROGRAM ELEMENT, PROJECT, TASK AREA & WORK UNIT NUMBERS AO 4397/3, 3D60, 62714
11. CONTROLLING OFFICE NAME AND ADDRESS AFOSR, Bolling Air Force Base, Washington, D.C. 20332		12. REPORT DATE 28 February 1985
		13. NUMBER OF PAGES 68
14. MONITORING AGENCY NAME & ADDRESS(if different from Controlling Office) DARPA Arlington VA.		15. SECURITY CLASS. (of this report) Unclassified
		15a. DECLASSIFICATION/DOWNGRADING SCHEDULE

16. DISTRIBUTION STATEMENT (of this Report)

Approved for public release; distribution unlimited.

17. DISTRIBUTION STATEMENT (of the abstract entered in Block 20, if different from Report)

18. SUPPLEMENTARY NOTES

from 20

19. KEY WORDS (Continue on reverse side if necessary and identify by block number)

nuclear explosion,
seismic data,
surface waves,
source mechanisms

20. ABSTRACT (Continue on reverse side if necessary and identify by block number)

The general objective of the research supported by this grant has been a better definition of the explosion and earthquake source processes. Specific elements of the research program and a list of 19 different research contributions which have been completed during the grant period are contained in Section II.

Love and Rayleigh wave group velocities for the Tibetan Plateau have been used to infer crustal velocities for that region. Results include

next page

DD FORM 1 JAN 73 1473 EDITION OF 1 NOV 65 IS OBSOLETE

UNCLASSIFIED

SECURITY CLASSIFICATION OF THIS PAGE (When Data Entered)

CONTNENTS

II

REVIEW OF RESEARCH COMPLETED

The general objective of the research effort has been a better definition of the explosion and earthquake source processes. Specific elements of the research program are: 1) recording of broadband data from events at the Nevada Test Site; 2) analysis of the coherence of ground motion near explosions and earthquakes; 3) study of the relative isotropic and non-isotropic components of explosive sources through the application of moment tensor inversion techniques; 4) analysis of regional surface wave data in order to obtain models for the velocity and attenuation of the crust; and 5) archival of near and regional data sets which are of value to the general discrimination problem.

Table 1 contains a list of research contributions which have been completed during the grant period. All of these have been published except for items 3 and 4. Item 3 is a condensed version of material that appeared in our Technical Report for 01 October 1982 - 31 October 1983, so it is not reporduced here. Item 4 is included as Section III of this report.

During the grant period two explosions at NTS were recorded with our digital network. The Coalora event was detonated in Yucca Flat on February 11, 1983. It was recorded by 10 three-component accelerometer stations in the distance range 0.7-5.4 km and an azimuthal range of 150 degrees. The Chancellor event was detonated in Pahute Mesa on September 1, 1983. It was recorded by 11 three-component accelerometer stations in the distance range 1.8-9.7 km and an azimuthal range of 360 degrees.

11) McLaughlin, K. L., L. R. Johnson, T. V. McEvilly, Two-dimensional array measurements of near-source ground accelerations, Bull. Seism. Soc. Am., 73, 349-375, 1983.

12) O'Connell, D. R., P. E. Murtha, Source parameters of Coalinga aftershocks from the UC Berkeley portable digital array, EOS, 64, 748, 1983.

13) Pomeror, P. W., W. J. Best, T. V. McEvilly, Test ban treaty verification with regional data - a review, Bull. Seism. Soc. Am., 72, S89-S129, 1982.

14) Scheiner, J. E., Attenuation near the San Andreas fault zone from reflection data, Earthquake Notes, 54, 51, 1983.

15) Scheiner, J. E., T. V. McEvilly, Seismic attenuation and crustal structure near the San Andreas fault zone from deep reflection profiling, Earthquake Notes, 55, 10, 1984.

16) Stump, B. W., L. R. Johnson, Near-field source characterization of contained nuclear explosions in tuff, Geophys. J. R. Astr. Soc., 74, 1-26, 1984.

17) Trali, D. M., Tau estimates of lateral variations in mantle P-wave velocities, EOS, 64, 755, 1983.

18) Trali, D. M., L. R. Johnson, Lower mantle tau estimates for a regionalized earth, EOS, 65, 999, 1984.

19) Vasco, D. W., T. V. McEvilly, J. E. Peterson, Polarization analysis and the effect of lithology on the coda of two earthquakes in the San Andreas fault zone, central California, Earthquake Notes, 54, 35, 1983.

THE TIBETAN LITHOSPHERE: NEW SEISMIC DATA FAVOR AN OLD MODEL

Kin-Yip Chun
Thomas V. McEvilly

Seismographic Station
and
Earth Sciences Division
Lawrence Berkeley Laboratory

University of California
Berkeley, California 94720

Introduction

The continuing convergence of the Indian and Eurasian continents since the Eocene-Oligocene transition some 40 Myr ago has produced a zone of deformation extending as much as 3000 km northeast of the Himalayan range.[1] Rising to 5 km average elevation over an area almost the size of the entire U.S. western cordillera, the Tibetan Plateau is one of the most conspicuous land features on this planet. Geophysicists debate whether its underlying 70-km-thick crust[2–6] was created by underthrusting of the Indian subcontinent[7,8] (the underthrusting model), by horizontal shortening with thickening under N-S compression[9] (the contraction model), or by some other process.

Chinese and French scientists recently reported[10] new paleomagnetic data suggesting that the Tibetan landmass is made up of several continental and/or island arc fragments which were progressively attached to the Eurasian continent between late Paleozoic and late Cretaceous[11,12] (the accretion model). Crustal shortening by the associated underthrusting brings the crustal thickness to 70 km, twice the normal continental value. The contraction and accretion models emphasize

are known.

Tibetan crustal velocity models have been derived mainly from seismic Rayleigh and Love surface wave dispersion data.[2-6] Recent investigations[17,18] have quantified model parameter resolutions with formal geophysical inversion techniques concluding, generally, that the Tibetan crust is about 70 km thick, with a V_S in the lower half crust averaging 3.60 km/sec, a value sufficiently low to be considered indicative of partial melting.[5] These surface wave studies all use mixed-path data, i.e., wave propagation paths sampling both Tibetan and neighboring crust, in which the fraction of Tibetan path rarely exceeds 2/3 the total path. Numerical simulations readily demonstrate that formal resolution analyses fail when plane-layered models are applied to a mixed-structure having large lateral variations in properties.

Refraction studies[5] yield high upper mantle V_P and V_S values of 8.12 ± 0.06 km/sec and 4.80 ± 1.0 km/sec, respectively. High frequency Sn (0.5 to 2 Hz), a seismic phase considered diagnostic of physical properties in the uppermost mantle, is found to propagate efficiently beneath Tibet and the Indian Shield.[19] This is in marked contrast to poor Sn propagation seen in regions of high heat flow and recent volcanism, such as the western U.S. Basin and Range province, the East African Rift system[20] and the northern Iranian Plateau.[21]

Taken together, these results from previous surface wave and body wave studies imply an intriguing phenomenon in which a thickened, hot Tibetan crust apparently overlies a cold, shield-like mantle.

invariant from one propagation path to the other. Slowness data in the 8-100 sec period-range were fitted by least-squares, as shown in Fig. 3a, for each period. The reciprocal of the slowness intercept gives the desired pure-path Tibetan group velocity. Figures 3b and 3c summarize the resulting pure-path and several representative mixed-path group velocity curves for Rayleigh and Love waves. A TPF of 0.5 (50% Tibetan path) is typical for the data used in most previous surface wave studies of Tibet. From Figures 3b and 3c, relative to our estimated pure-path velocities, the non regionalized group velocities are in error by about 0.4 and 0.2 km/sec, respectively, for Rayleigh and Love waves. Inversion of such mixed-path data will lead to serious errors in the resulting structure.

The validity of our regionalization scheme can be tested with independent regionally recorded mixed-path data sets, by the ability of the standard curves in Figures 3b,c and the Tibetan boundary in Figure 1 to predict the independent data set. To illustrate, we consider the conveniently tabulated mixed-path group velocity data for Rayleigh and Love waves from a previous study[4] involving 17 paths along which the average TPF is 0.66, possibly the largest of any previous Tibetan studies. When the results in Figures 3b,c are used to construct Rayleigh and Love wave standard curves with a TPF of 0.66, they are found to fit the corresponding mixed-path data[4] quite closely, with a root-mean-squares difference of about 0.03 km/sec. The velocity model determined from the TPF=0.66 mixed-path data is shown in Figure 4 labeled TP4.

In the bottom 40 km of the Tibetan crust, where previous mixed-path studies have persistently reported an anomalously low 3.6 km/sec average velocity, we find V_S of 3.88 ± 0.08 km/sec, which compares with the 3.85 km/sec value found in the lower crust of the Canadian Shield.[32]

Our surface wave data do not constrain details in the upper mantle beneath the thick Tibetan crust; the inversion yields a 4.50-4.55 km/sec average upper mantle V_S, a value in qualitative agreement with analyses of travel-time residuals which indicates that the mean velocity in the topmost 200-300 km of the Tibetan mantle must be anomalously low.[5,33] This contrasts with the high 8.12 km/sec V_P and 4.80 km/sec V_S obtained under Tibet in mantle refraction studies.[5] Taken together, these results imply a thin, high-velocity mantle lid extending no deeper than about 100 km beneath the surface.[5]

Our proposed crust-mantle shear velocity model TP100 of the Tibetan Plateau is shown in Figure 4, along with the calculated and the observed surface wave data. By normal standards the fit is excellent. Velocity uncertainties are given for the layer thicknesses shown.

Temperature at Base of Crust

Recent research[34] yields a correlation between the upper mantle compressional velocity P_n and estimated temperature T_m at the base of the crust. The equation $P_m = 8.456 - 0.000729\ T_m$, where P_m is the measured P_n corrected to a 35 km reference depth using a pressure derivative of 0.015 km/sec per 100 MPa, is based on an exhaustive study covering numerous distinct tectonic provinces across North America.[34] Using 8.12 ± 0.06 km/sec as the Tibetan P_n, this equation gives a T_m, at the

develop under shear in the lowest part of the overlying Eurasian crust, and water forced from the uppermost part of the underthrusted Indian continental crust enhances the cracks by hydraulic fracturing or by chemical corrosion.[38] Pore pressure then rises as a direct result of shear-straining and the local heating resulting from it.

Beneath the Himalayas and southern Tibet, where the lower crust is recently emplaced, the amount of water being released should be relatively significant, lowering the sliding friction in the fault zone. Some of the water may find its way to the surface through fissures, creating hot-springs found in that region. Beneath northern Tibet, in contrast, lies the dry, long-heated leading edge of the underthrusted Indian lithosphere, where a combination of pre-heating and increased sliding friction may cause local partial melting. This south-to-north gradation can explain both the only active volcanism (Fig. 1) and the near absence of geothermal activity in the Kun-Lun.

A Missing Granitic Layer?

The uniformly high, 3.88 km/sec V_S in the 40-km-thick lower crustal section does not appear compatible with the continental underthrusting model. Apparently lacking is a typical granitic layer ($V_S \sim 3.65$ km/sec) expected in its upper portion. A case can be made, however, for its upper half being a granitic layer in disguise.

As a result of underthrusting, the average lithostatic pressure in the granitic layer (assuming a 20 km thickness) of the Indian crust is increased from 300 to 1400 MPa; and the temperature to no more than 500°C in the available time since large-scale underthrusting commenced in Miocene time. Mean pressure and temperature derivatives of 0.0194

discriminate among competing models for the development of the Tibetan Plateau. Major results are:

1. The crust beneath Tibet is 74 ± 10 km thick with average V_S of 3.54 km/sec.
2. A prominent shear wave low velocity zone is seen in the depth range of 24-34 km, where V_S is approximately 2.64 km/sec.
3. V_S in the lower 40 km of the crust is uniformly high (3.88 ± 0.08 km/sec).
4. The LVZ, overlain by an upper crust with properties similar to the Basin and Range or the Andes, and underlain by a high-velocity, presumably cool, lower crust, is better explained by high pore water pressure than by partial melt.
5. The high V_S values in the lower crust, along with previous body wave studies of upper mantle P_n and S_n, imply the presence of an unusually cool region in the depth range 50-100 km.

These results may be interpreted to indicate that the Eurasian geotherm was probably similar to that of the Basin and Range until large-scale continental underthrusting began during early Miocene time. The underthrusting Indian lithosphere some 120 km thick[43] was warmed from above by the heat generated in the fault zone and from below by the heat flux from the underlying asthenosphere. The short time available does not allow thermal equilibration near its mid-section.

We present the schematic drawing in Fig. 5 to describe our tectonic model of Tibet consistent with the above conclusions on the evolution of the plateau.

Figure Captions

Figure 1. Surfacc wave paths used to study the crust-mantle structure beneath the Tibetan Plateau (shaded region). The epicenters of earthquakes used in this study are indicated as small filled circles, and WWSSN stations are shown as open circles with code letters. Active volcanoes are marked as larger filled circles. Map based on Molnar and Tapponnier.[1]

Figure 2. Long-period surface wave seismograms (above) and the results of the moving-window group velocity analysis (below) for a 0.75 fraction of Tibetan Plateau path (TPF) and a 0.27 TPF path, left (Rayleigh Wave) and right (Love Wave), respectively. Limits of the vertical bars and shading represent two different *energy contour* levels.

Figure 3. Pure-path group velocity determination. Figure 3a demonstrates for two periods the least-squares determination of pure-path slowness values, the intercepts which are shown with their uncertainties (two standard deviations). Slownesses are plotted for a given period as a function of non-Tibetan path percentage. Figures 3b and 3c show the resulting pure-path Rayleigh and Love wave group velocity curves so determined, along with some mixed-path curves.

References

1. Molnar, P. & Tapponnier, P., *Science* 189, 419-426 (1975).
2. Gupta, H.K. & Narain, H., *Bull. Seism. Soc. Am.* 57, 235-248 (1967).
3. Tung, J.P. & Teng, T.L., *EOS Trans. AGU* 55, 359 (1974).
4. Chun, K.Y. & Yoshii, T., *Bull. Seism. Soc. Am.* 67, 735-750 (1977).
5. Chen, W.P. & Molnar, P., *J. Geophys. Res.* 86, 5937-5962 (1981).
6. Romanowicz, B.A., *J. Geophys. Res.* 87, 6865-6883 (1982).
7. Argand, E., *Int. Geol. Congr. Rep. Sess.* 13, 171-372 (1924).
8. Powell, C. McA. & Conaghan, P.J., *Earth Planet. Sci. Letters* 20, 1-12 (1973).
9. Dewey, J.F. & Burke, K.C.A., *J. Geol.* 81, 683-692 (1973).
10. Allégre, C.J. et al., *Nature* 3.7, 17-36 (1984).
11. Chang, C. & Cheng, H., *Sci. Sinica* 16, 257-265 (1973); in Proc. Symp. on Qinghai-Xizang (Tibet) Plateau. (Gordon & Breach, New York, 1981).
12. Chang, C. & Pan, Y., Proc. Symp. on Qinghai-Xizang (Tibet) Plateau, 2, 1-18 (Gordon & Breach, New York, 1981).
13. Jin, C., Proc. Symp. on Qinghai-Xizang (Tibet) Plateau, 2, 433-450 (Gordon & Breach, New York, 1981).
14. Toksöz, M.N. & Bird, P., *Tectonophysics* 41, 181-193 (1977).
15. Spencer, J.W., Jr. & Nur, A.M., *J. Geophys. Res.* 81, 899-904 (1976).
16. Lin, W.N., Ph.D. Thesis, Univ. of California, Berkeley (1976).
17. Pines, I., Teng, T.L. & Rosenthal, R., *J. Geophys. Res.* 85, 3829-3844 (1980).

37. Lachenbruch, A.H. & Sass, J.H., *Geol. Soc. Am. Memo.* 152, 209-250 (1978).

38. Scholz, C.H., *J. Geophys. Res.* 73, 3295-3302 (1968).

39. Francheteau, J. et al., *Nature* 307, 32-36 (1984).

40. Li, J.J. et al., Proc. Symp. on Qinghai-Xizang (Tibet) Plateau, 2, 111-118 (Gordon & Breach, New York, 1981).

41. Zhang, Q.S. et al., Proc. Symp. on Qinghai-Xizang (Tibet) Plateau, 2, 103-110 (Gordon & Breach, New York, 1981).

42. Chun, K.Y. & McEvilly, T.V., *Trans. AGU* 64, 860 (1983).

43. Toksöz, M.N., Chinnery, M.A. & Anderson, D.L., *Geophys. J. Roy. Astron. Soc.* 13, 31-39 (1967).

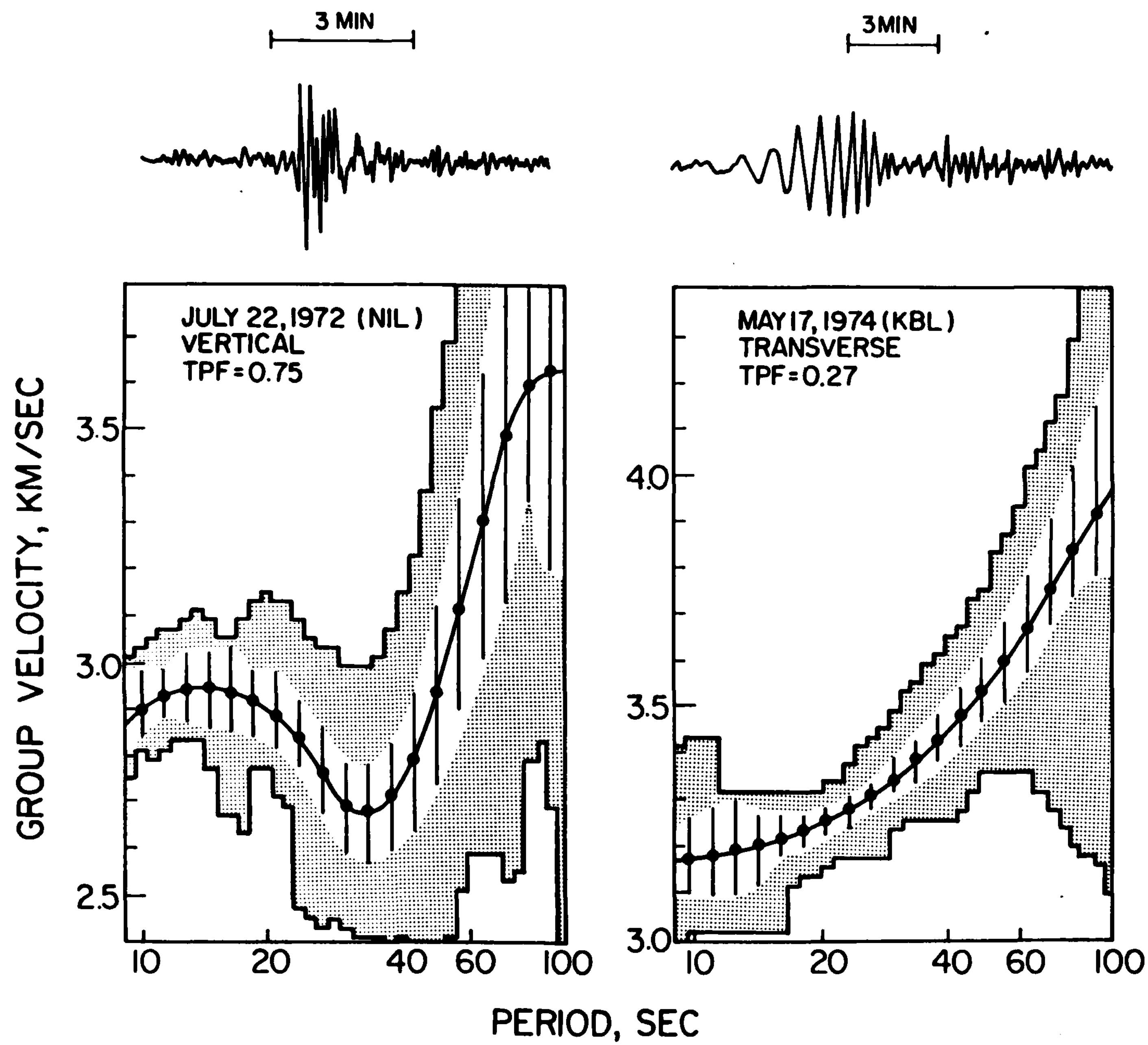
3 MIN
3MIN
JULY 22, 1972 (NIL)
VERTICAL
TPF = 0.75
MAY 17, 1974 (KBL)
TRANSVERSE
TPF = 0.27
GROUP VELOCITY, KM/SEC
3.5
3.0
2.5
4.0
3.5
3.0
10
20
40
60
100
PERIOD, SEC

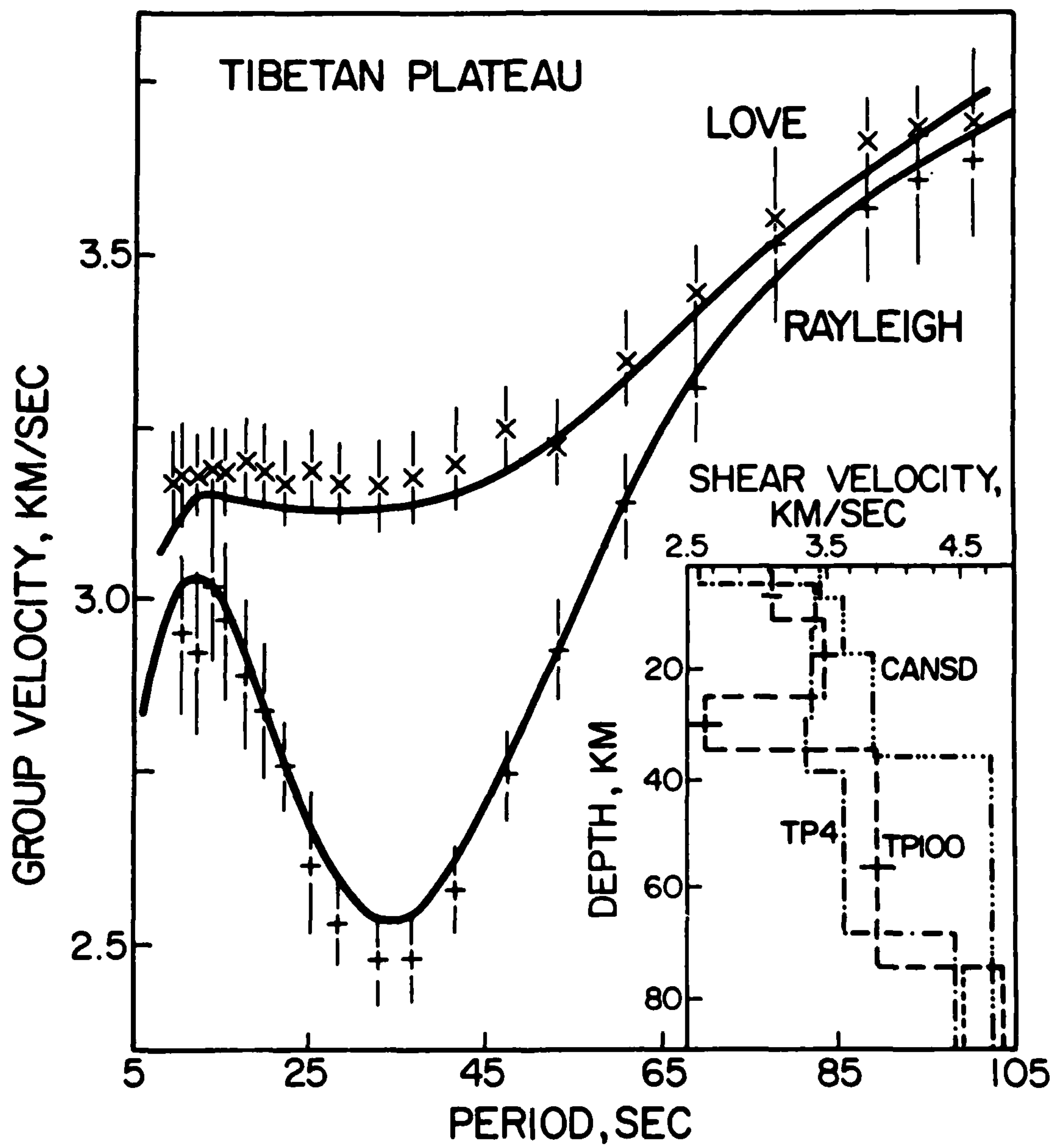
TIBETAN PLATEAU
LOVE
RAYLEIGH
GROUP VELOCITY, KM/SEC
3.5
3.0
2.5
5
25
45
65
85
105
PERIOD, SEC
SHEAR VELOCITY, KM/SEC
2.5
3.5
4.5
DEPTH, KM
20
40
60
80
CANSD
TP4
TP100

Figure 4

REGIONAL STUDIES WITH BROADBAND DATA

by

Lane R. Johnson

Thomas V. McEvilly

Seismographic Station
Dept. of Geology and Geophysics
University of California
Berkeley, CA 94720

Introduction

VELA-sponsored research at Berkeley began around 1960 with the program of Dr. Don Tocher and Prof. Perry Byerly to expand their central California network of the UC Seismographic Stations, and to link for the first time such a network by FM telemetry to a central recording site (see Figure 1). Their purpose was to improve research capabilities for studying the mechanisms of local earthquakes. Shortly thereafter, with AFOSR support, the BKS WWSSN station was installed, and a three-component, broadband (flat velocity response, 0.03-10 Hz, dual gains) station was installed at BRK with continuous slow-speed (0.06 ips) FM recording on magnetic tape. In 1964 the tape recording system was expanded to handle also six of the short-period telemetered stations.

During the subsequent two decades leading to today, the AFOSR-supported research program has concentrated on investigations into the source mechanisms of earthquakes and explosions, along with techniques for discriminating between them. From the start, the research was based largely upon the new broadband data being acquired by the network from local earthquakes and from underground explosions at the nearby Nevada Test Site (NTS), although some studies used teleseismic data. Promising results of early discrimination studies with NTS data, along with source studies of moderate-size central California earthquakes, led to further expansion of the broadband stations to BKS, JAS, WDC and SAO (see Figure 2). Early work on near-field observations of earthquakes, at Berkeley and elsewhere, led to initiation in the early seventies of the AFOSR "Near Field Program", a multi-institution co-operative study of the Bear Valley - Stone Canyon seismogenic zone

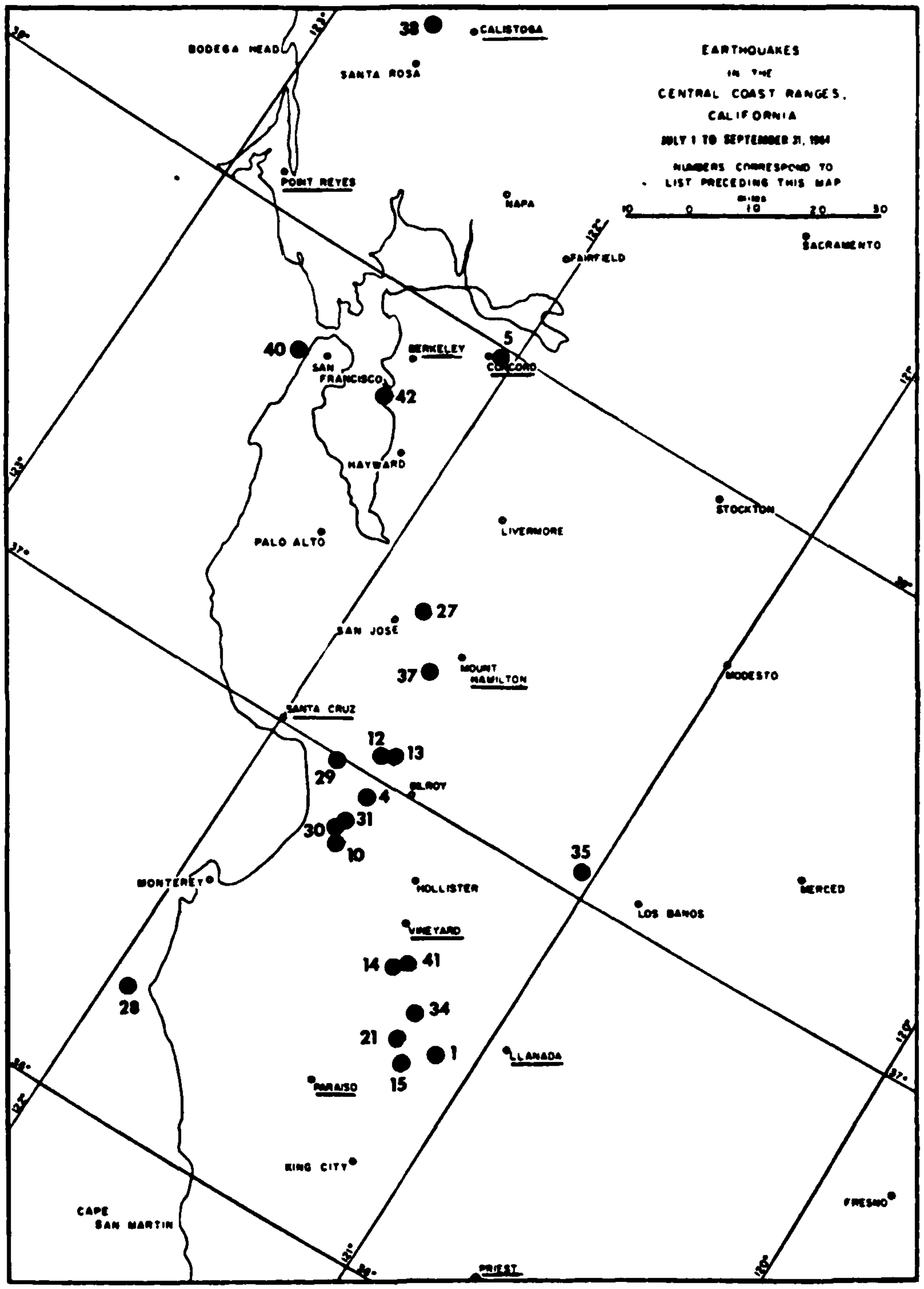

Figure 1. UC Seismographic Stations network in 1964 with third quarter seismicity. Stations of AFOSR-supported telemetered network are underlined.

Spectral Evidence for Fault Rupture Parameters

The M_L 5.5 1966 Parkfield earthquake was well recorded on the BRK broadband system, providing data for many investigation since. In one study the Love wave spectra were analyzed for propagation of the rupturing fault surface. This early application of directivity effects compared Love wave spectra for five of the larger earthquakes in the sequence, shown in Figure 1. The spectra, seen in Figure 2, reveal clear notches at periods consistent with a fault rupture length of about 30 km and a rupture velocity of 2.2 km/sec. The four smaller events (M_L 3.8 to 5.1) are quite similar, scaling at 10-20 sec periods closely with M_L. The 5.5 M_L mainshock at these periods scales to a much larger value than its measured M_L, as seen in Figure 2, which represents an early demonstration of the M_L saturation phenomenon.

Short Period Discriminant at Regional Distances

A spectral ratio method was shown to successfully discriminate between underground explosions and natural earthquakes when applied to the Pg phase at regional distances. The data set included 69 events recorded at the Berkeley network station JAS in the distance range 250 to 500 km and the magnitude range 2.8 to 4.5 (Table 1). The Pg spectral ratio (0.6-1.25 Hz)/(1.35-2.0 Hz) shows explosions and natural earthquakes to separate into distinct sets for magnitude greater than 3.2, with explosions relatively richer in the high frequency band. An interesting result was that the spectra of afterevents of large explosions resemble the spectra of explosions more than that of natural earthquakes. However, these afterevents appear to be more like natural earthquakes when the m_b:M_s discriminant is applied.

Table 1 (*continued*)

No.	Type	Date	OT (GMT)	Lat. (N)	Long. (W)	Δ (km) from JAS	$M^{(4)}$	Spectral ratio (P_g)	Comments
54	c	1968 December 12	15 20 00	(37·1)	(116·0)	(390)	3·8	1·36	(4)
55	c	1968 December 19	17 30 22·8	37·2	116·5	360	3·4	1·24	(3)—BENHAM 'Afterevent'
56	c	1968 December 19	19 18 19·6	37·3	116·4	360	3·5	0·48	(3)—BENHAM 'Afterevent'
57	c	1968 December 19	19 54 01·2	37·2	116·5	360	3·4	0·39	(3)—BENHAM 'Afterevent'
58	c	1968 December 19	22 23 26·3	37·2	116·5	360	3·6	1·06	(3)—BENHAM 'Afterevent' (collapse?
59	c	1968 December 20	20 08 20·4	37·2	116·5	360	3·8	0·61	(3)—BENHAM 'Afterevent'
60	c	1968 December 21	00 14 25·2	37·3	116·5	360	4·3	—	(3)—BENHAM 'Afterevent)
61	c	1969 January 6	06 34 14·5	37·3	116·5	360	4·2	—	(3)—BENHAM 'Afterevent'
62	c	1969 January 10	09 41 21·5 *	37·2	116·5	360	3·9	1·72	(3)—BENHAM 'Afterevent'
63	c	1969 January 10	17 01 44·5	37·2	116·5	360	3·8	2·82	(3)—BENHAM 'Afterevent'
64	c	1969 January 10	17 14 17·2	37·2	116·5	360	3·8	0·88	(3)—BENHAM 'Afterevent'
65	c	1969 March 18	14 40 02·7	37·2	116·0	400	3·8	0·69	(3)
66	c	1969 September 16	15 43 49·2	37·2	116·5	360	3·8	2·38	(3)—JORUM 'Afterevent'
67	c	1969 September 16	16 23 53·8	37·3	116·5	360	3·9	1·39	(3)—JORUM 'Afterevent'
68	c	1969 September 16	17 31 14·7	37·3	116·5	360	4·0	3·44	(3)—JORUM 'Afterevent'
69	c	1969 September 16	18 15 39·3	37·3	116·5	360	3·8	1·52	(3)—JORUM 'Afterevent'

(1) Magnitudes based on P_n and P_g amplitudes at JAS. The scale is based on Wood–Anderson magnitudes at BRK for larger events.

(2) Personal communication, Don Springer, 1970. The letter designations (Y) and (P) indicate the test areas Yucca Flat and Pahute Mesa, respectively; (R) indicates an elongated explosive charge was detonated as a 'row shot' at Buckboard Mesa. The origin times of collapses may be uncertain by a few seconds.

(3) U.S.C.G.S. hypocentre.

(4) Arrival times at the Berkeley net indicate NTS hypocentre. Δ = 360 or 390 km is assumed for purposes of attentuation and magnitude calculations.

* Arrival times available for this event are inconsistent so that the epicentral distance is uncertain. The magnitude thus may be as large as 3·2 if the epicentre is 500 km from JAS. The error in the attenuation correction due to the epicentral uncertainty is not significant.

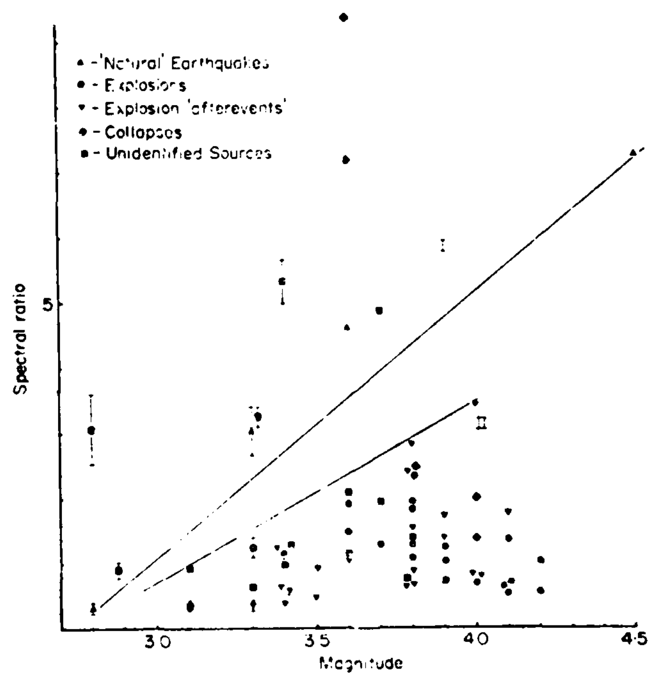

Fig. 1 P_g spectral ratio of vertical surface displacement, corrected for attenuation with $Q = 400$, at JAS for events within 100 km of NTS. I and II denote the earthquake and explosion fields, respectively.

Seismographic Stations

Station	Type of instrument	Location	Epicentral dist. from MILROW (deg)	Azimuth from MILROW (deg)
Belleview, Florida (BEFL)	Geotech 18300 (CANNIKIN)	28° 54′ 19″ N; 82 03 52 W	73·1	64·8
Berkeley, California (BRK)	Press Ewing LP (CANNIKIN)	37 52 ·4N; 122 15 ·6W	42·7	84·8
Houlton, Maine (HNME)	Portable Benioff (MILROW) Geotech 18300 (CANNIKIN)	46 09 43 N; 67 59 09 W	66·9	44·0
Kanab, Utah (KNUT)	Large Benioff (MILROW) Geotech 18300 (CANNIKIN)	37 01 22 N; 112 49 39 W	49·1	79·1
Las Cruces, New Mexico (LCNM)	Portable Benioff (MILROW)	32 24 08 N; 106 35 58 W	56·0	79·1
Priest, California (PRI)	Portable Benioff (CANNIKIN)	36 08 ·5N; 120 39 ·9W	44·8	85·6
Red Lake, Ontario (RKON)	Portable Benioff (MILROW) Geotech 18300 (CANNIKIN)	50 50 20 N; 93 40 20 W	51·5	54·0
San Jose, Texas (SJTX)	Geotech 18300 (MILROW) Geotech 18300 (CANNIKIN)	27 36 43 N; 98 18 46 W	64·4	77·2

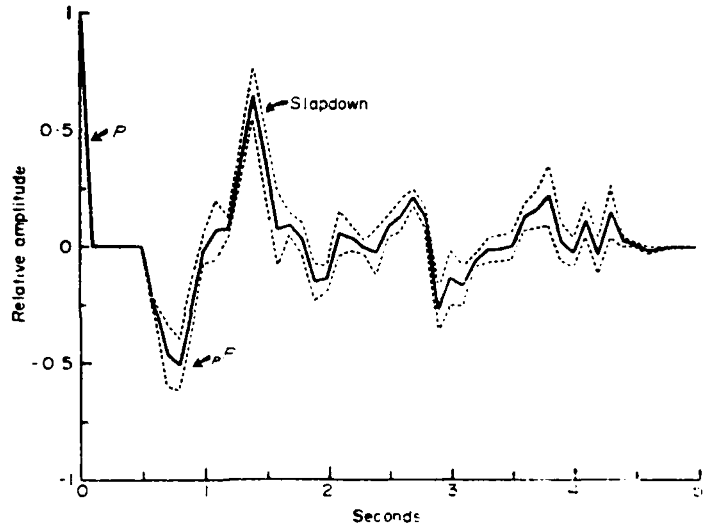

FIG. 1 Mean impulse train (solid line) ± its standard deviation (dashed line) for MILROW. Impulse trains from KNUT, HNME, LCNM and RKON were used to compute the mean.

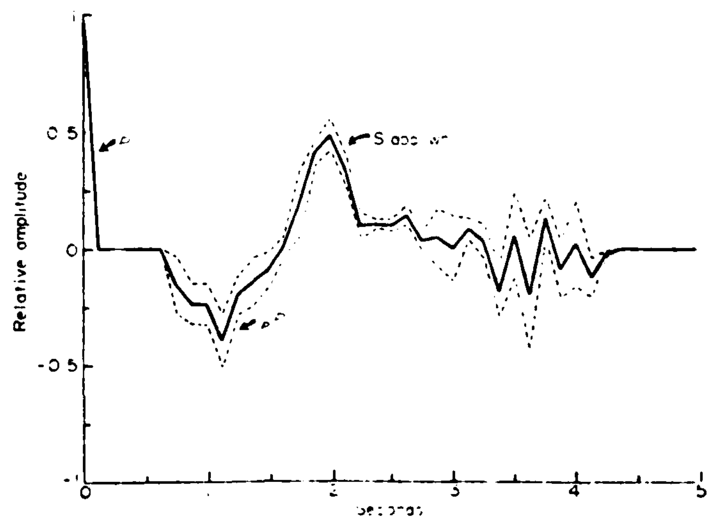

FIG. 2 Mean impulse train (solid line) ± its standard deviation (dashed line) for CANNIKIN. Impulse trains from HNME, KNUT, SJTX and BRK were used to compute the mean.

Table 1

Data on events used in this study

Event	Location	Time	Date	Amplitude Rayleigh	P_n	M_L
Explosions						
PINSTRIPE	NTS	1838	1966 April 25	4·0	0·8	4·5
CYCLAMEN	NTS	1400	1966 May 5	1·0	0·4	4·2
DUMONT	NTS	1356	1966 May 19	100·0	18·0	5·5
DISCUS THROWER	NTS	2000	1966 May 27	7·5	4·0	4·7
PUCE	NTS	1430	1966 June 10	2·0	0·7	4·3
KANAKEE	NTS	1803	1966 June 15	2·5	0·8	4·8
VULCAN	NTS	1713	1966 June 25	2·0	1·0	4·5
HALFBEAK	NTS	2215	1966 June 30	500·0	30·0	5·9
NEWPOINT	NTS	1750	1966 December 13	1·0	0·3	4·5
GREELEY	NTS	1530	1966 December 20	1440·0	60·0	6·2
AGILE	NTS	1850	1967 February 23	80·0	12·0	5·5
MICKEY	NTS	1340	1967 May 10	6·5	1·5	4·6
COMMODORE	NTS	1500	1967 May 20	180·0	20·0	5·6
SCOTCH	NTS	1400	1967 May 23	240·0	14·5	5·6
KNICKERBOCKER	NTS	1500	1967 May 26	124·0	9·0	5·2
MIDI MIST	NTS	1600	1967 June 26	5·5	2·0	4·7
UMBER	NTS	1125	1967 June 29	1·0	0·6	4·6
YARD	NTS	1345	1967 September 7	12·5	3·5	5·0
KNOX	NTS	1530	1968 February 21	70·0	19·0	5·6
DORSAL FIN	NTS	1708	1968 February 29	6·0	3·0	4·6
NOOR	NTS	1400	1968 April 10	2·0	1·0	4·3
SHUFFLE	NTS	1405	1968 April 18	8·0	4·0	5·2
SCROLL	NTS	1702	1968 April 23	2·5	0·5	4·5
BOXCAR	NTS	1500	1968 April 26	1960·0	80·0	6·3
DIANA MOON	NTS	1630	1968 August 27	1·0	0·5	4·0
NOGGIN	NTS	1400	1968 September 6	82·0	17·0	5·5
HUDSON SEAL	NTS	1705	1968 September 24	5·5	3·5	4·6
CREW	NTS	1515	1968 November 4	4·0	3·0	4·6
SCHOONER	NTS	1600	1968 December 8	12·0	2·5	5·1
BENHAM	NTS	1630	1968 December 19	2720·0	48·0	6·2
WINESKIN	NTS	1930	1969 January 15	26·0	6·0	5·0
BLENTON-THISTLE	NTS	1700	1969 April 30	30·0	5·0	5·0
JORUM	NTS	1430	1969 September 16	1240·0	100·0	6·2
PIPKIN	NTS	1430	1969 October 8	112·0	12·5	5·5
CRUET	NTS	1930	1969 October 29	1·0	0·7	4·4
CYATHUS	NTS	1424	1970 March 6	0·5	1·0	4·2
SHAPER	NTS	2305	1970 March 23	54·0	8·0	5·4
HANDLEY	NTS	1900	1970 March 26	1360·0	120·0	6·2
CORNICE	NTS	1330	1970 May 15	20·0	8·0	5·0
MORRONES	NTS	1415	1970 May 21	11·2	1·7	5·0

Table 1 (*continued*)

Event	Location	Time	Date	Rayleigh	P_n	M_L
HUDSON MOON	NTS	1416	1970 May 26	2·5	1·2	4·2
FLASK	NTS	1500	1970 May 26	30·0	14·5	5·2
BANEBERRY	NTS	1530	1970 December 18	7·0	4·5	4·9
EMBUDD	NTS	1450	1971 June 16	2·0	0·5	4·2
LAGUNA	NTS	1530	1971 June 23	2·4	1·1	4·5
HAREBELL	NTS	1400	1971 June 24	8·3	3·5	4·9
Unidentified*	NTS	1830	1971 June 29	4·7	2·7	4·4
Unidentified*	NTS	1400	1971 September 22	0·5	0·6	3·9
PEDERNAL	NTS	1400	1971 September 29	1·5	0·5	4·1
CATHAY	NTS	1430	1971 October 8	1·5	0·5	4·7
Unidentified*	NTS	1430	1971 October 14	1·0	0·3	4·0
Explosion Collapses						
DUMONT	NTS	1537	1966 May 19	14·0	0·4	4·5
HALFBEAK	NTS	0133	1966 July 1	21·0	0·5	4·2
AGILE	NTS	2111	1967 February 23	10·0	0·3	4·3
YARD	NTS	1425	1967 September 7	7·5	0·2	4·1
KNOX	NTS	1634	1968 February 21	15·0	0·3	4·4
BOXCAR	NTS	1635	1968 April 26	15·0	0·5	5·0
BOXCAR	NTS	1645	1968 April 26	21·0	0·2	4·8
BENHAM	NTS	2224	1968 December 19	47·0	0·3	4·6
JORUM	NTS	1544	1969 September 16	4·0	0·6	3·8
JORUM	NTS	1623	1969 September 16	6·0	0·4	3·7
JORUM	NTS	1731	1969 September 16	13·0	0·5	4·3
JORUM	NTS	1815	1969 September 16	15·0	0·3	4·2
SHAPER	NTS	0115	1970 March 24	6·4	0·2	4·2
HAREBELL	NTS	1441	1971 June 24	5·5	0·3	3·8
Explosion Aftershocks						
SCOTCH	NTS	2014	1967 May 23	2·5	0·3	3·8
BOXCAR	NTS	1532	1968 April 26	112·0	2·5	5·3
BENHAM	NTS	0014	1968 December 21	26·0	1·3	4·8
BENHAM	NTS	1810	1968 December 22	7·0	0·5	4·2
BENHAM	NTS	0634	1969 January 06	11·0	0·8	4·6
BENHAM	NTS	0941	1969 January 10	10·0	0·4	4·6
BENHAM	NTS	1701	1969 January 10	6·0	0·2	4·4
BENHAM	NTS	1714	1969 January 10	6·0	0·3	4·5
Earthquakes						
CENTRAL NEVADA	38·6 N 116·2 W	1321	1968 May 22	36·0	0·8	4·9
ADEL, OREGON	42·2 N 119·8 W	1255	1968 May 28	3·5	0·3	3·8
ADEL, OREGON	42·3 N 119·8 W	0037	1968 May 30	22·0	0·5	4·7
SANTA BARBARA	34·3 N 119·7 W	1912	1968 June 29	148·0	4·0	4·9
SANTA BARBARA	34·2 N 119·6 W	2036	1968 June 29	9·0	0·5	3·8
SANTA BARBARA	34·2 N 119·7 W	0036	1968 July 5	22·0	0·5	4·2
SANTA BARBARA	34·1 N 119·7 W	0045	1968 July 5	720·0	14·0	5·5
NORTHERN NEVADA	41·0 N 117·4 W	1402	1968 June 16	62·0	2·0	5·2
SANTA BARBARA	34·2 N 119·8 W	1433	1968 July 7	60·0	2·0	4·5
SAN FERNANDO	34·4 N 118·4 W	1401	1971 February 9	7520·0	10·0	6·5
SAN FERNANDO	34·4 N 118·4 W	0517	1971 February 10	18·0	0·8	4·6
NTS	36·9 N 116·0 W	1758	1971 August 5	10·0	0·7	4·2

* Unidentified NTS events listed with explosions on basis of Rayleigh-P_n ratios.

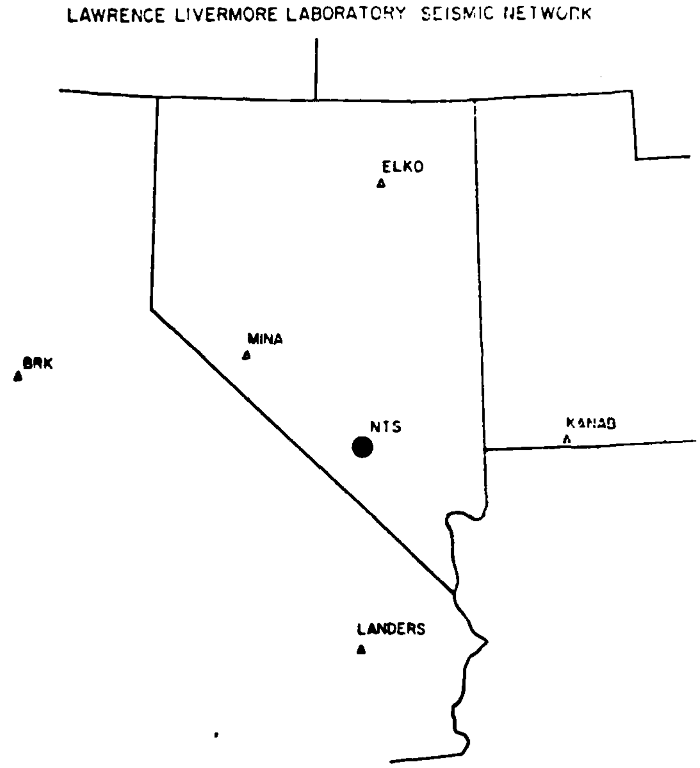

FIG. 1. Stations of the LLL network (open triangles) and the Berkeley (BRK) observatory.

Broadband Studies of Earthquakes in the Near Field

Broadband recordings (0.03 to 10 Hz) in the near field (2 to 40 km) were used to study a series of earthquakes along the San Andreas fault in central California. Special broadband instruments were operated on both sides of the fault at the San Andreas Geophysical Observatory (SAGO). The 13 earthquakes used in the study are listed in Table 1 and plotted in Figure 1. Spectra were used to estimate scalar moments (Figure 2) and establish a relationship between moment and local magnitude (Figure 3). The near field terms of the elastic displacement field caused by an earthquake were clearly present on the seismograms (Figure 5) and at near stations could be reasonably well modeled by a point dislocation source in a homogeneous halfspace (Figures 4 and 5), although the effects of tilt on the seismometers also had to be included.

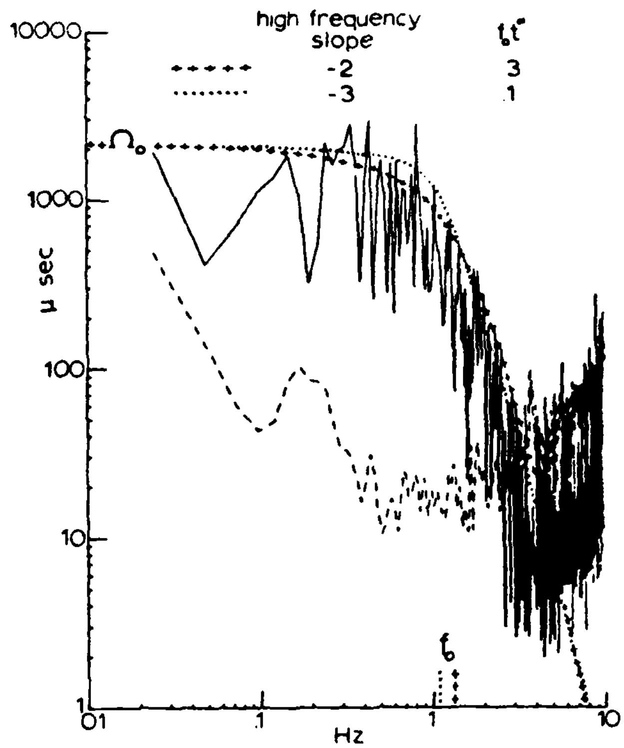

FIG. 2 Example illustrating two different estimates of the low-frequency level Ω_0 and the corner frequency f_0 of the spectrum from the NS component at SAGO-East from event 6 (Table 1).

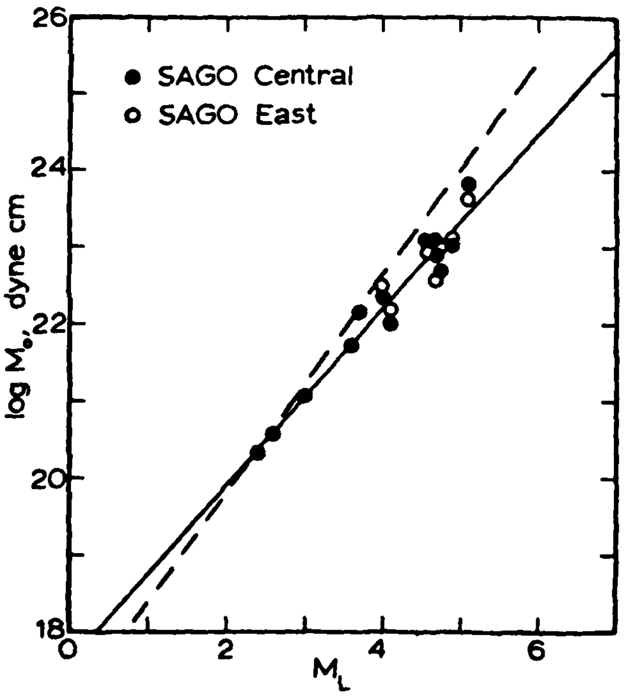

FIG. 3 Relation between seismic moment and magnitude. The solid line was fit to the data points by linear regression and the dashed line is from Wyss and Brune (1968). The SAGO-East values have been divided by a factor of 3 to remove an amplification effect.

Near Field Project

The "Near Field Project" grew out of some of the problems that became apparent at the Woods Hole meeting on seismic discrimination in 1970. Because the type of high quality data necessary to test various theoretical models of an earthquake was not available at that time, a cooperative experiment was designed to trap a moderate size earthquake within a network of stations designed to provide data over a large range of frequency, azimuth, and distance. The Stone Canyon-Bear Valley section of the San Andreas fault in central California was selected as the target area, and U.C. Berkeley had the responsibility of developing and installing a network of three-component broadband seismographs. Both acceleration and displacement were recorded and an effective bandwidth of 0.02 to 50 Hz was achieved (Figure 2).

The 9 stations of the network were installed in early 1973 and remained operational until early 1977. Figure 1 shows the locations of the stations and the epicenters of 3 earthquakes which provided useable data. Figure 3 shows the recordings of ground acceleration from the magnitude 3.3 event on July 6, 1974, obtained at an epicentral distance of 2 km. The clear separation of P and S waves, the short duration of the phases, the high frequencies, and the rather large accelerations for an event of this size are all of interest. Figure 4 shows the recordings of ground displacement as the same station from the same event. Here we see the large effect which can be introduced by ground tilt at stations in the near field.

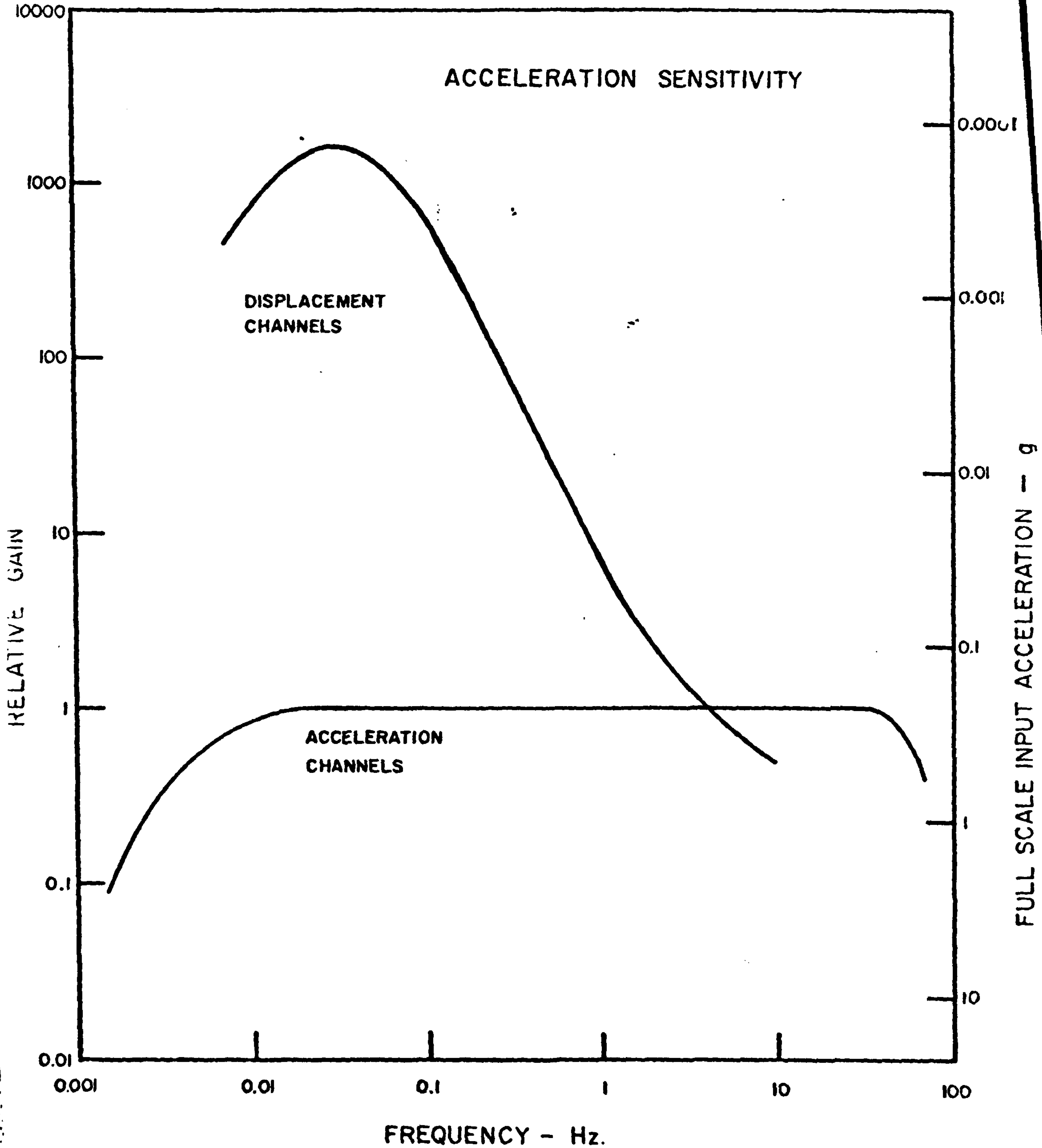

Figure 2. The system response functions of the acceleration and displacement

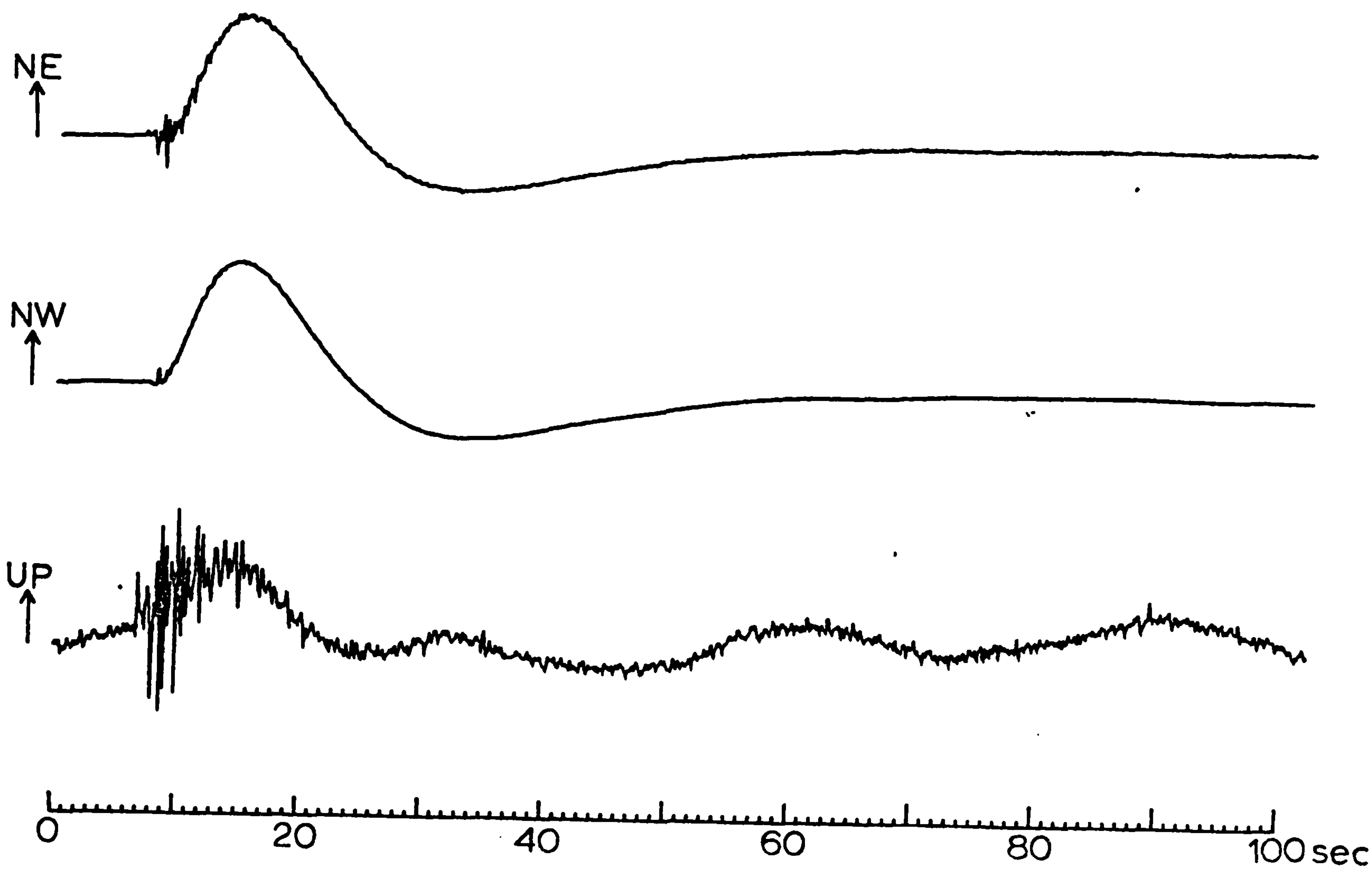

Figure 4. The outputs of the displacement channels at station number 2 for the earthquake of 6 July 1974 after being passed through a four-pole low-pass filter with a corner frequency at 4 Hz. The maximum displacements on the NE, NW, and Z channels are 3220 u, 7720 u, and 340 u, respectively.

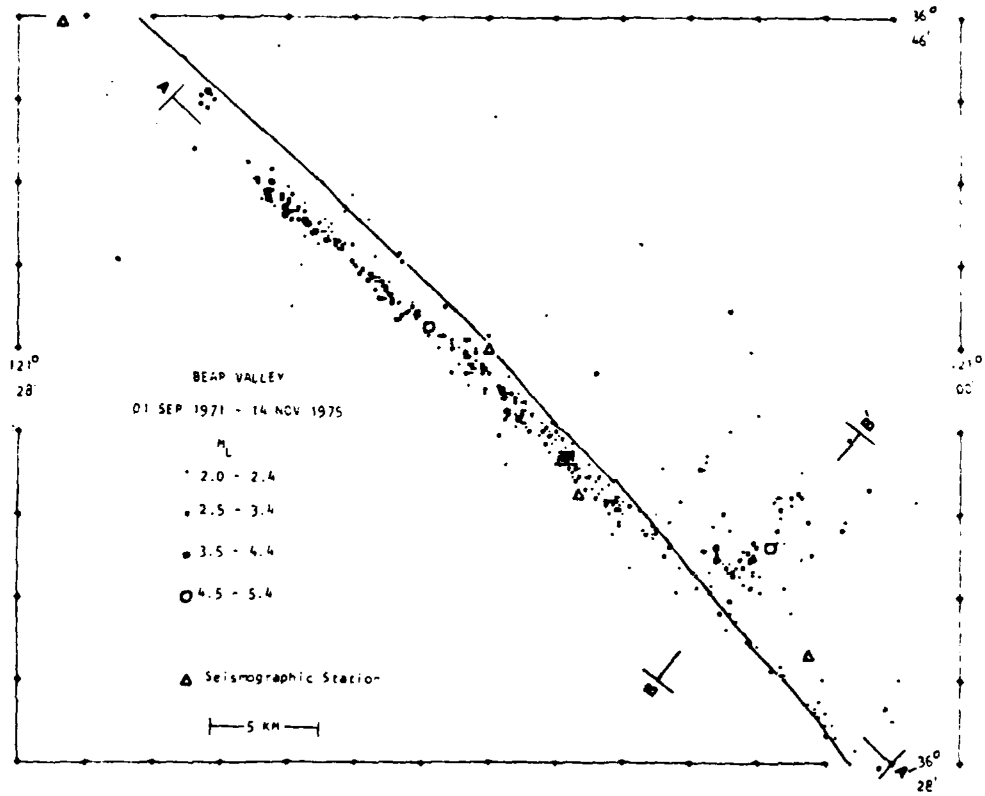

FIG. 1. Seismicity of Bear Valley/Stone Canyon study region, 1971–1975.

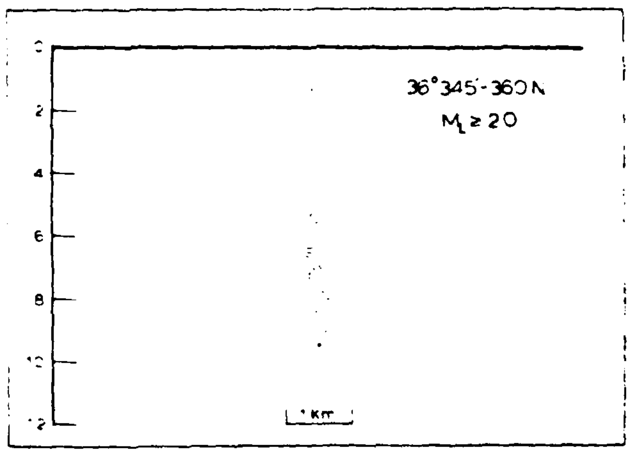

FIG. 2. Cross section across fault at 36°34.5′ to 36.0′, showing narrow vertical fault plane.

Near Field Experiments at the Nevada Test Site

Beginning in 1969, U.C. Berkeley has conducted an experimental program of recording explosions at the Nevada Test Site. Table 1 lists the 13 events which have been recorded so far. These experiments have included events in both Yucca Valley and Pahute Mesa. They have also included a variety of recording arrangements, ranging from arcs at a single distance, networks containing stations at a variety of azimuths and distances, one-dimensional arrays, and two-dimensional arrays. Figure 1 shows the events and stations for the experiments at Pahute Mesa. The combined data set from this series of experiments is now large enough to permit systematic studies of propagation and site effects, particularly for the Pahute Mesa region.

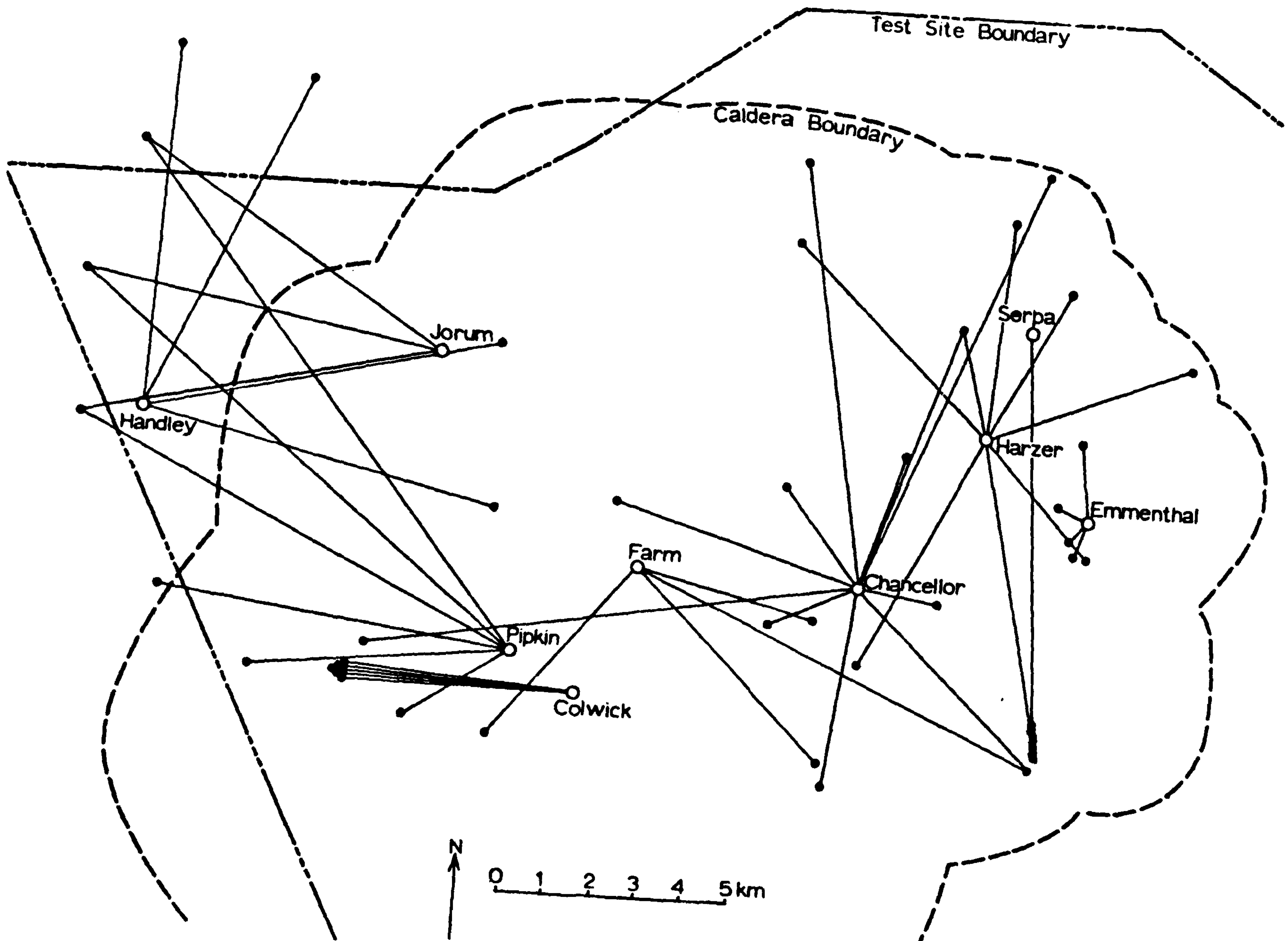

Figure 1. Explosion sites (open circles with names) and respective recording sites (filled circles) for near field data acquisition at Pahute Mesa.

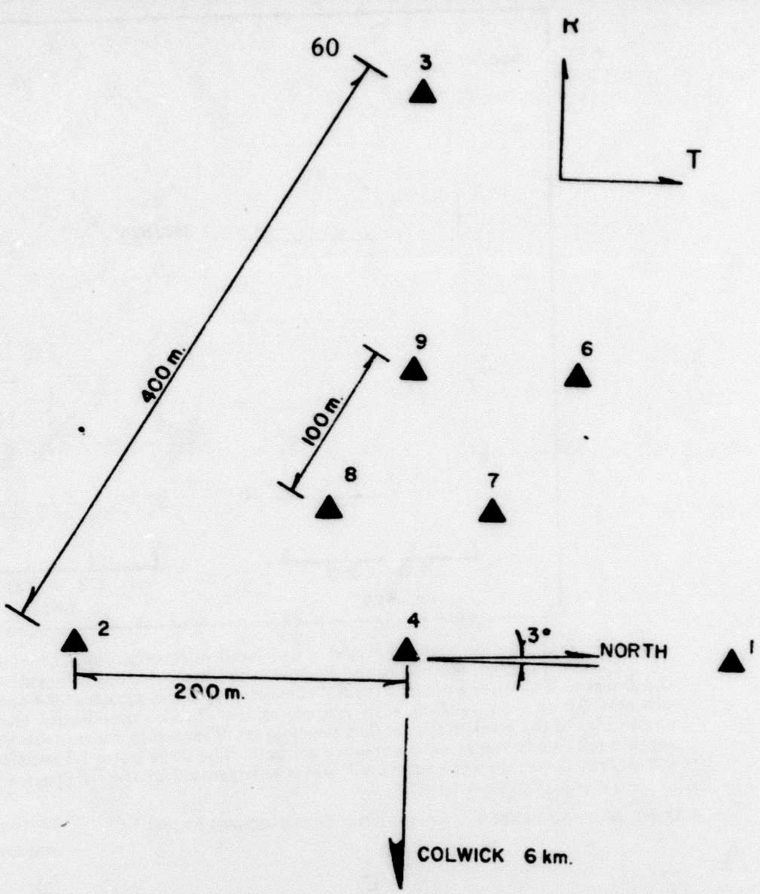

FIG. 1 The eight stations of the Colwick array arranged in nested triangles of 400, 200, and 100 m. Each station consisted of a three-component accelerometer package and a digital event recorder. Vertical is up, radial is away, and transverse is clockwise from radial. Colwick was 6 km 93°E of N from the array.

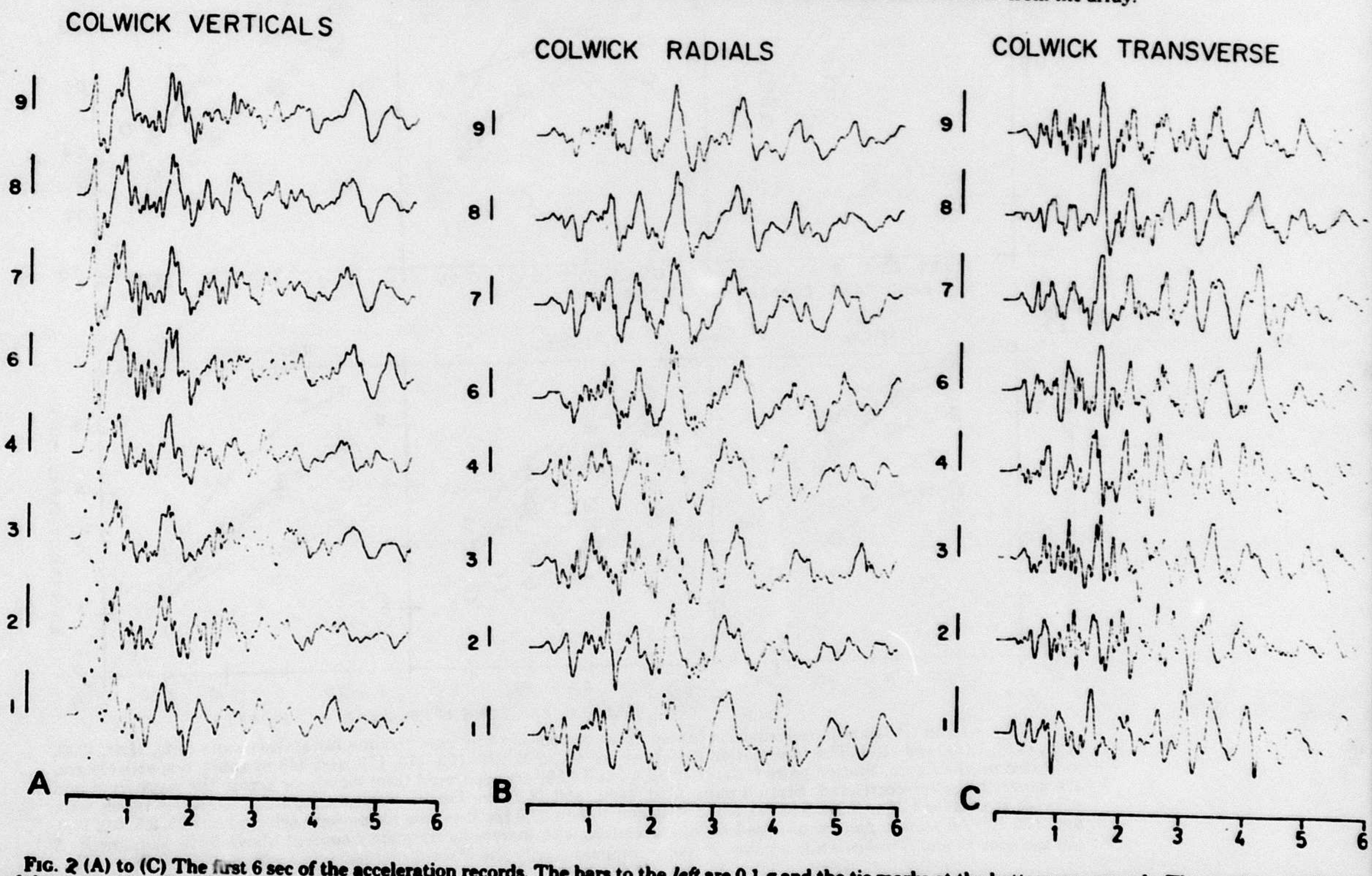

FIG. 2 (A) to (C) The first 6 sec of the acceleration records. The bars to the *left* are 0.1 *g* and the tic marks at the bottom are seconds. The numbers to the *left* of the traces identify the station numbers.

NTS Area Crustal Velocity and Q Structure from Broadband Surface Waves

An application of the phase-matched filtering process to multimode Rayleigh and Love waves from NTS explosions recorded at the four LLNL broadband stations (Figure 1, Table 1) proved surprisingly effective in extracting pure-path group velocities. Fundamental mode Love and Rayleigh waves and first shear mode of the Rayleigh wave were observed, yielding data in the period range 2 to 50 seconds. Data for the Landers station are shown in Figure 2, in which observations are given as dots. These velocities are the lowest found for the Basin - Range, apparently because they represent the shortest observation paths ever used, thus avoiding upward bias of true velocities inherent in the averaging process which is involved in using long paths. Inversion for structure yields the NTS-Landers model of Figure 3, and the calculated dispersion curves are shown as solid curves in Figure 2. Statistically significant differences in models for the four paths are seen, apparently correlating with the regional variations in heat flow. Pure-path amplitudes are also extracted by the phase-matched filtering, and they allow estimation of a regional Q structure which, while highly uncertain, indicates Q values greater than 100 in the upper 5-10 km, and less than 50 below that depth. These new data on Basin - Range structure will be used to improve Greens Functions for explosion source inversion from regional data sets.

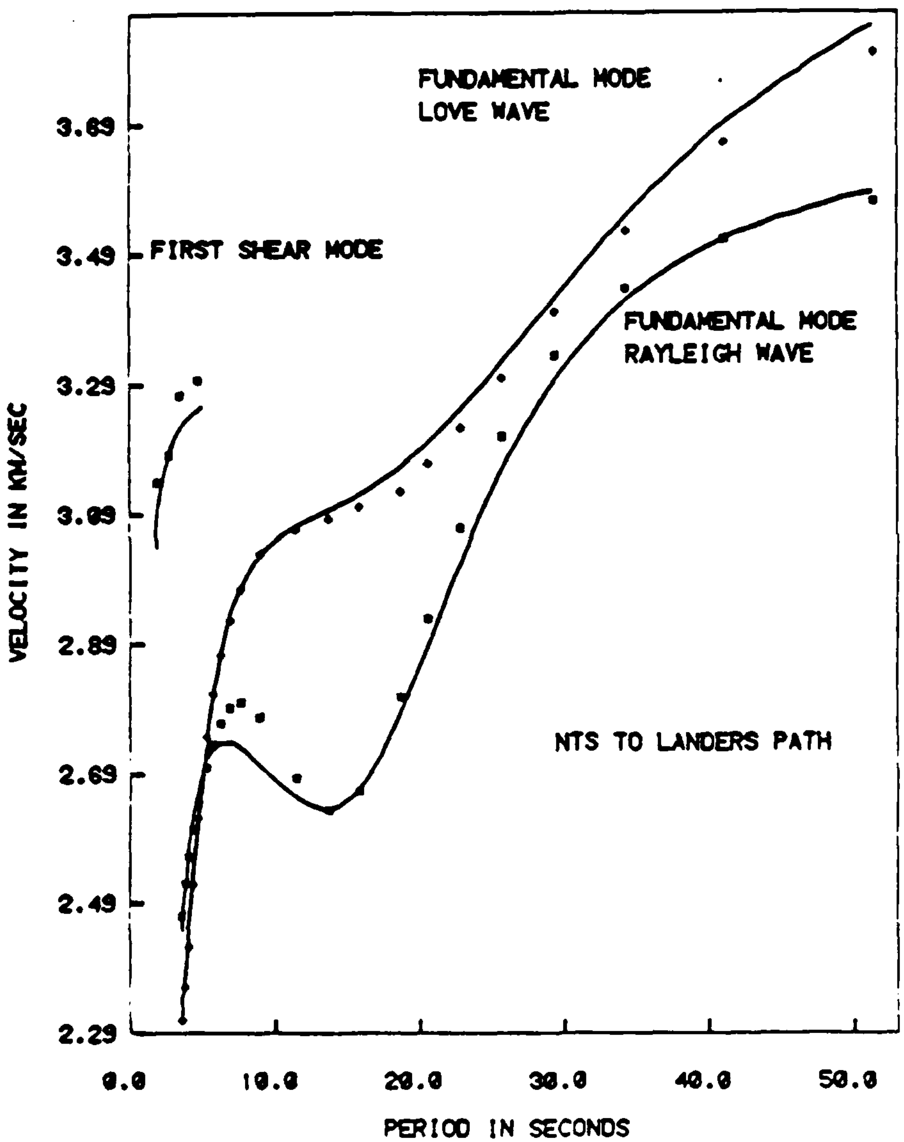

Figure 2. Observed (dots) and calculated dispersion.

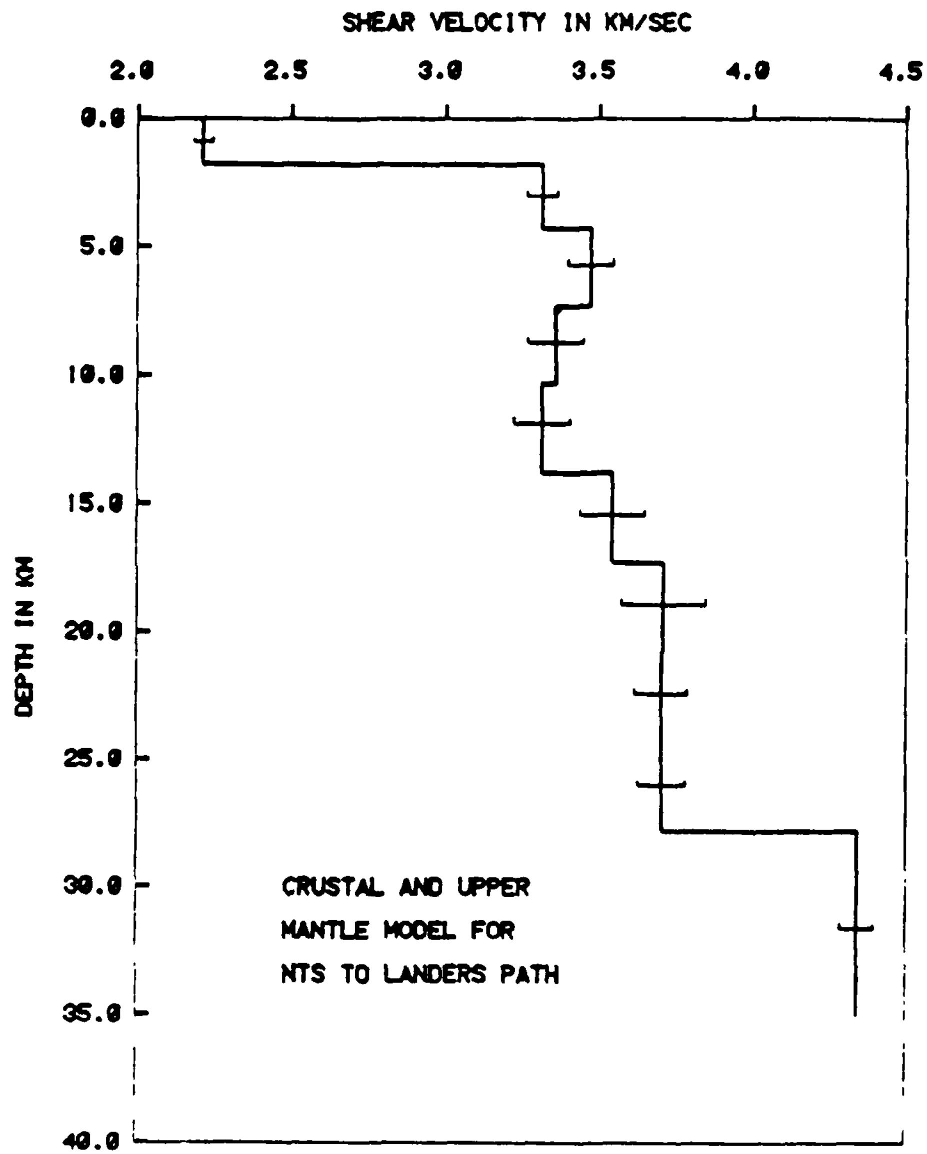

Figure 3. NTS - Landers model based upon inversion of data in Figure 2.

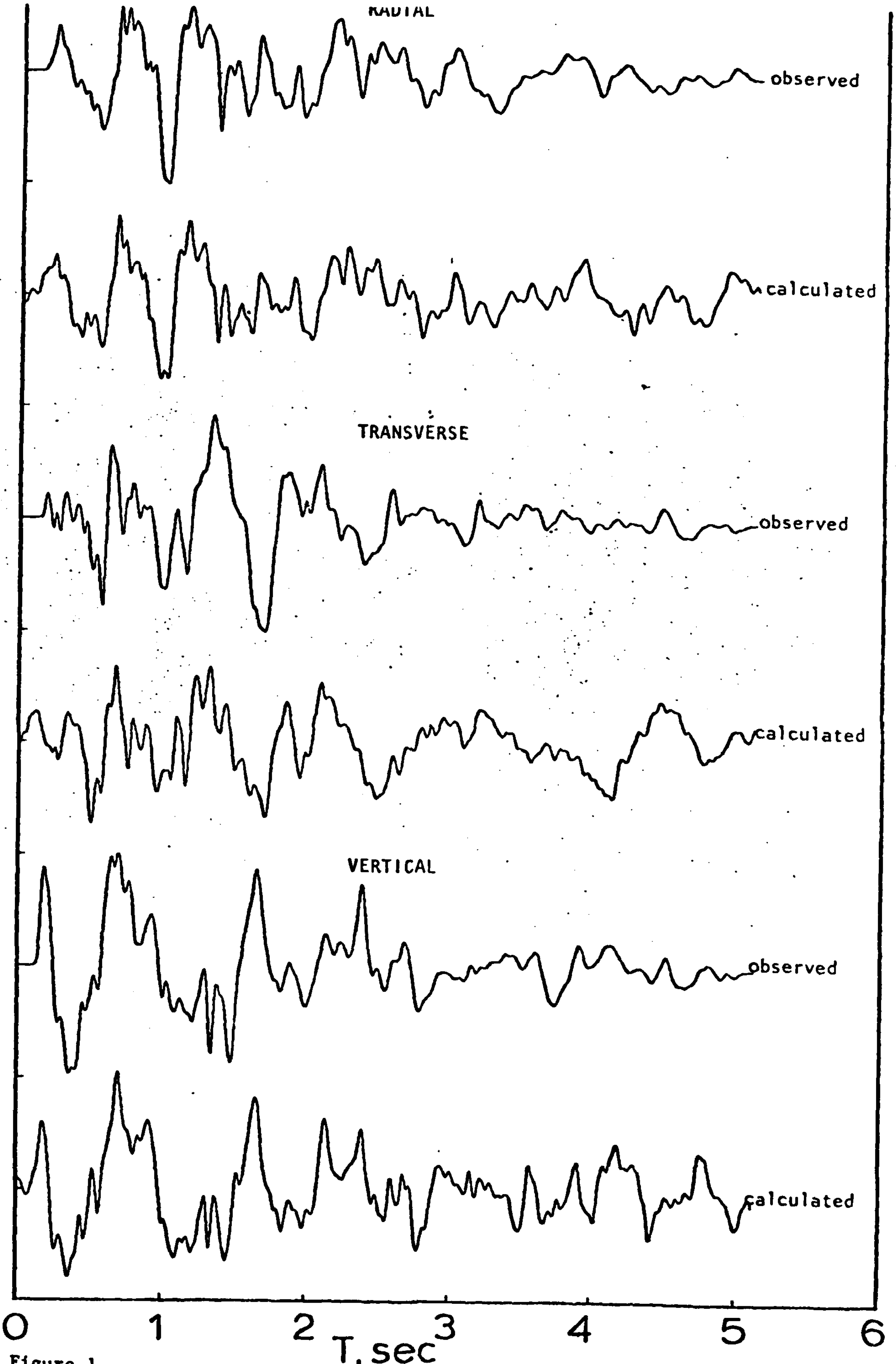

Figure 1.
Observed and calcualted accelerations for station H9 of HARZER.

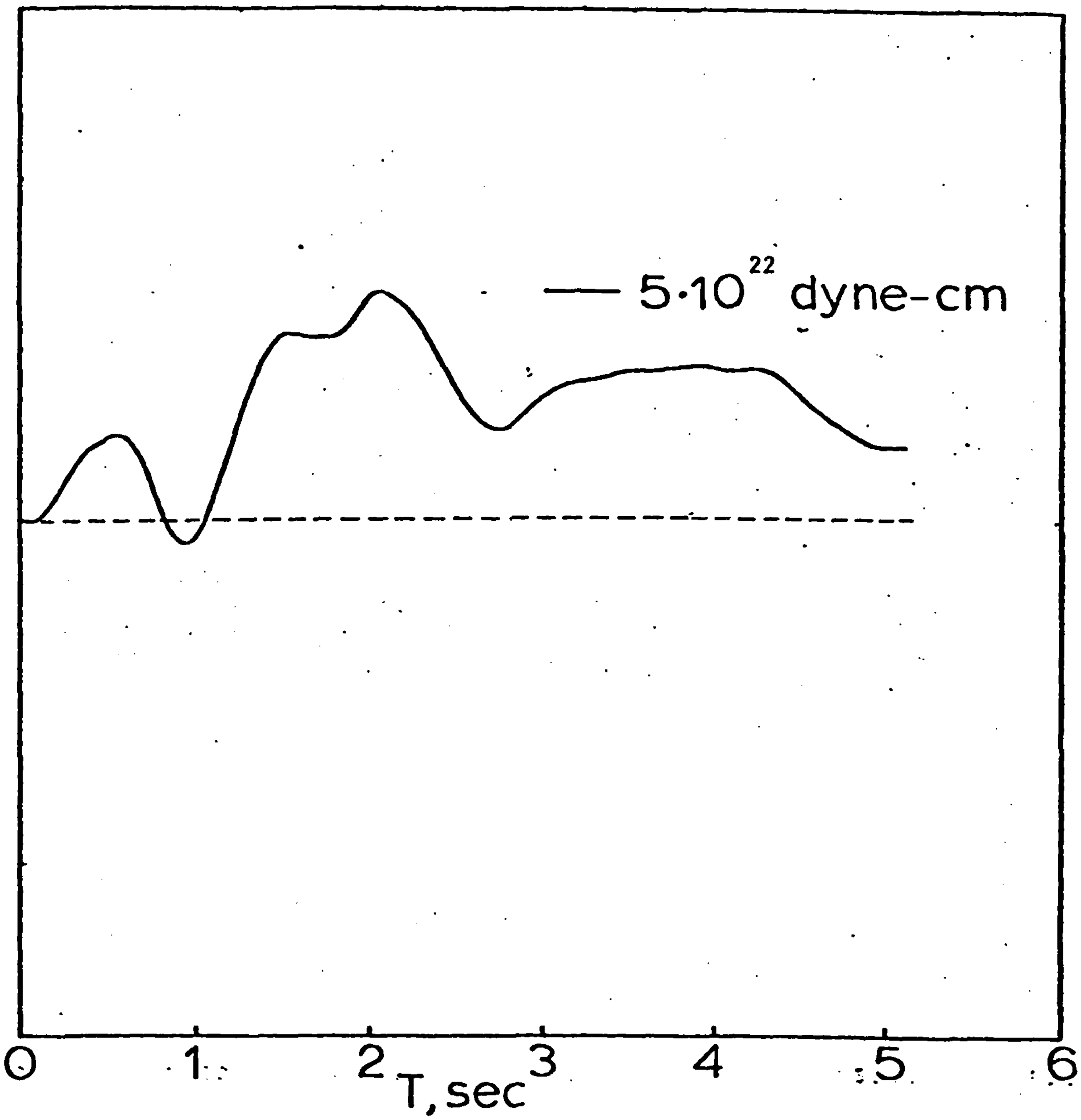

Figure 3.
Estimate of the isotropic part of the first-degree moment tensor of the explosion HARZER.

All the event pages scanned, but no odd pages.